

# CM<sup>2</sup> MAGAZINE



第 118 期



南方科技大学海洋磁学中心主编

<http://cm2.sustech.edu.cn/>

## 创刊词

海洋是生命的摇篮，是文明的纽带。地球上最早的生命诞生于海洋，海洋里的生命最终进化成了人类，人类的文化融合又通过海洋得以实现。人因海而兴。

人类对海洋的探索从未停止。从远古时代美丽的神话传说，到麦哲伦的全球航行，再到现代对大洋的科学钻探计划，海洋逐渐从人类敬畏崇拜幻想的精神寄托演变成可以开发利用与科学研究的客观存在。其中，上个世纪与太空探索同步发展的大洋科学钻探计划将人类对海洋的认知推向了崭新的纬度：深海（deep sea）与深时（deep time）。大洋钻探计划让人类知道，奔流不息的大海之下，埋藏的却是亿万年的地球历史。它们记录了地球板块的运动，从而使板块构造学说得到证实；它们记录了地球环境的演变，从而让古海洋学方兴未艾。

在探索海洋的悠久历史中，从大航海时代的导航，到大洋钻探计划中不可或缺的磁性地层学，磁学发挥了不可替代的作用。这不是偶然，因为从微观到宏观，磁性是最基本的物理属性之一，可以说，万物皆有磁性。基于课题组的学科背景和对海洋的理解，我们对海洋的探索以磁学为主要手段，海洋磁学中心因此而生。

海洋磁学中心，简称  $CM^2$ ，一为其全名“Centre for Marine Magnetism”的缩写，另者恰与爱因斯坦著名的质能方程  $E = MC^2$  对称，借以表达我们对科学巨匠的敬仰和对科学的不懈追求。

然而科学从来不是单打独斗的产物。我们以磁学为研究海洋的主攻利器，但绝不仅限于磁学。凡与磁学相关的领域均是我们关注的重点。为了跟踪反映国内外地球科学特别是与磁学有关的地球科学领域的最新研究进展，海洋磁学中心特地主办  $CM^2$  Magazine，以期与各位地球科学工作者相互交流学习、合作共进！

“海洋孕育了生命，联通了世界，促进了发展”。21世纪是海洋科学的时代，由陆向海，让我们携手迈进中国海洋科学的黄金时代。

## 目录

1. 早更新世时期岁差周期对北部冰盖的持续性影响 .....	2
2. 台湾海峡南部沙质海底地形相关的空间变异性 .....	6
3. 中国东南仙云洞在 Heinrich 4 期间记录的东亚夏季风的三阶段结构 .....	9
4. 地球构造碳输送带的演化 .....	13
5. 马里亚纳海沟沉积物中的磁性有孔虫特征 .....	15
6. 菲律宾海中部深海沉积物第四纪的磁性地层学和区域沉积动力学 .....	17
7. 泥盆纪是持续非均变古地磁场? .....	19
8. 伊比利亚半岛全新世人类活动对火灾的影响 .....	23
9. 相对海平面变化数据指示晚全新世 Pine Island Bay 并没有发生明显的冰盖变化 .....	25
10. 格陵兰 EastGRIP 冰芯的融化揭示了全新世温暖事件 .....	28

## 1. 早更新世时期岁差周期对北部冰盖的持续性影响

翻译人：仲义 zhongy@sustech.edu.cn



*Barker, A.D, Starr, A., van der Lubbe, J., et al. Persistent influence of precession on the northern ice sheet variability since the early Pleistocene [J] Science, 2022, 376, 961-967.*

<https://doi.org/10.1126/science.abm4033>

**摘要：**在一个百年万年前，全球冰盖比变化主要受到斜率周期的控制；然而，岁差周期的作用仍然未被厘清。利用北大西洋 1.7 百万年来冰筏碎屑的记录，作者发现冰筏碎屑开始在一个特定冰期旋回间（反映冰盖扩张特征），并与斜率周期的降低时间同步，而大量的冰盖消融事件则始终与岁差的最小值相关。进而，作者的研究结果表明，在中晚更新世时期，由岁差控制的消融时间和冰川终止期普遍存在关联。在此之前（增强），斜率周期本身足以结束一个冰期循环，而在 1 Ma 以后，随着北半球冰原的不断向南扩张，斜率周期失去了对冰川消退的主导作用。

**ABSTRACT:** Prior to ~1 million years ago (Ma), variations in global ice volume were dominated by changes in obliquity; however, the role of precession remains unresolved. Using a record of North Atlantic ice rafting spanning the past 1.7 million years, we find that the onset of ice rafting within a given glacial cycle (reflecting ice sheet expansion) consistently occurred during times of decreasing obliquity whereas mass ice wasting (ablation) events were consistently tied to minima in precession. Furthermore, our results suggest that the ubiquitous association between precession-driven mass wasting events and glacial termination is a distinct feature of the mid to late Pleistocene. Before then (increasing), obliquity alone was sufficient to end a glacial cycle, before losing its dominant grip on deglaciation with the southward extension of Northern Hemisphere ice sheets since ~1 Ma.

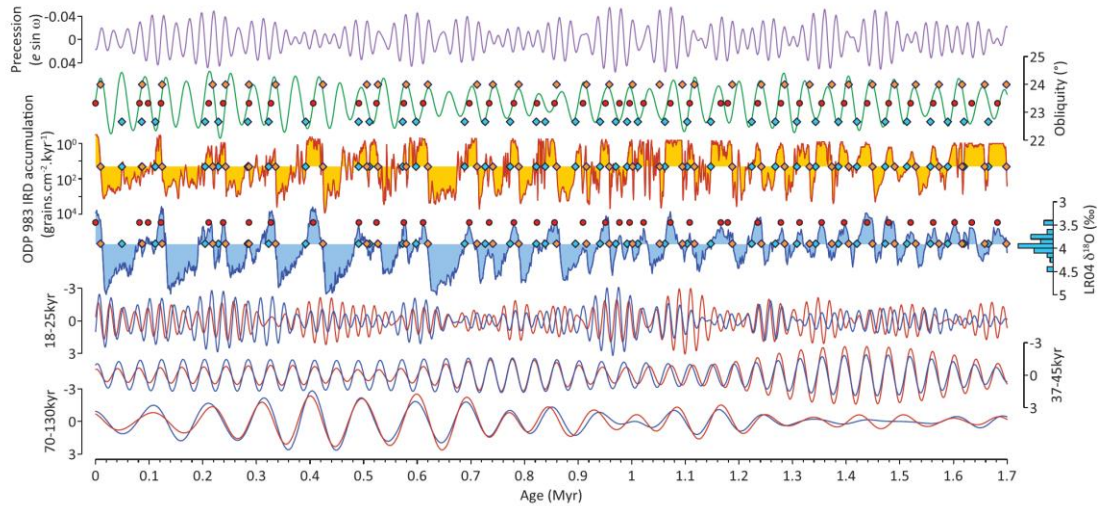


**Figure 1.** 1.7 Myr of ice rafting across the NE Atlantic. Red circles represent interglacials (as determined by our algorithm), blue diamonds represent onset of significant ice rafting (see orange-filled curve), and orange diamonds represent the end of TIR events. (Top to bottom) Precession, obliquity, IRD accumulation from ODP 983 on the LR04 age model (data have been smoothed and detrended to highlight intervals of significant ice rafting), the LR04 benthic stack (histogram represents values of  $d^{18}O$  at time of each IRD onset, mean =  $3.9 \pm 0.2\text{‰}$  as indicated by the horizontal fill threshold of the LR04 curve), 18 to 25 kyr, 37 to 45 kyr, and 70 to 130 kyr filter outputs of log IRD (red) and the LR04 stack (blue). Note coherence between the LR04 stack and log IRD on G-IG (41 kyr and subsequently  $\sim 100$  kyr) time scales throughout the past 1.7 Myr (see also fig. S17).

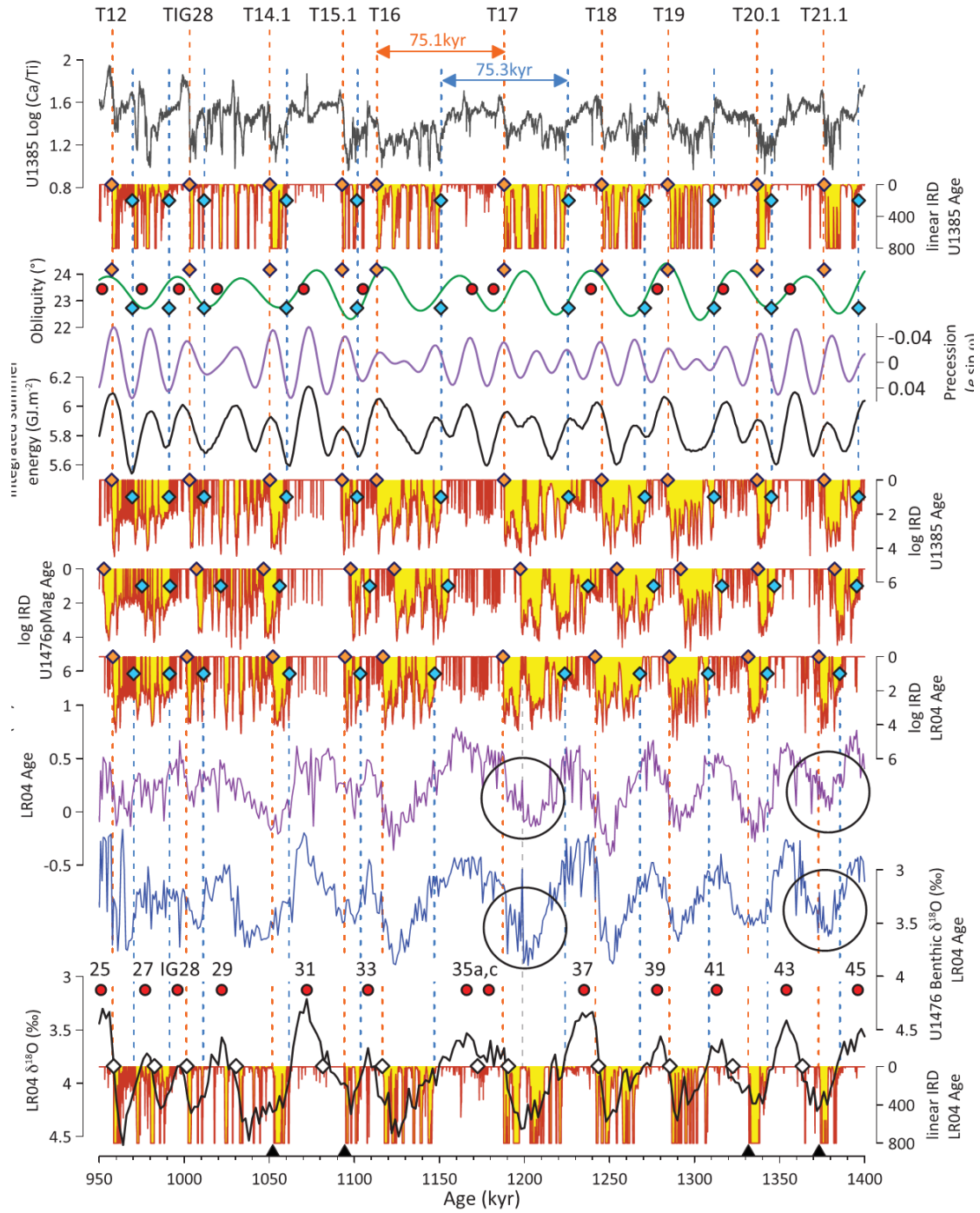


**Figure 2.** Obliquity loses its grip on deglaciation. Red circles represent interglacials (numbered; IG28 is a minimum in  $d^{18}O$  associated with MIS 28) (12), white diamonds are deglacial transitions with respect to  $d^{18}O$  (13), blue diamonds and vertical dashed lines represent onset of significant ice rafting, and orange diamonds (and lines) represent the end of TIR events. Orange and blue double-headed arrows highlight lengthening of glacial cycles to approximate multiples of the obliquity period following the late occurrence of T17 (see text and Fig. 3, right-hand panel, 1000 to 1250 ka).

(Top to bottom) Log (Ca/Ti) from U1385 ( 16), ODP 983 IRD accumulation on a linear scale (note cropped scale), obliquity and precession ( 26), integrated summer energy at 65°N, log IRD from ODP 983 on U1385, U1476pMag, and LR04 age models, benthic foraminiferal d<sup>13</sup>C and d<sup>18</sup>O from U1476 on its LR04 age model ( 13), the LR04 stack ( 14), and linear IRD on its LR04 age model. Black triangles (bottom) highlight “nonterminating” TIR events (identified as T14.1, T15.1, and so forth). Large black circles highlight shifts toward lighter values of benthic d<sup>18</sup>O in U1476 within glacial intervals. Both of these shifts are aligned with coincident features in the records of benthic d<sup>13</sup>C and IRD. Note that our algorithm does not assign a TIR event for T13 because IRD accumulation does not subside sufficiently before MIS 2

## 2. 台湾海峡南部沙质海底地形相关的空间变异性

翻译人: 刘伟 inewway@163.com



Shen X, Jian X, Li C, et al. *Submarine topography-related spatial variability of the southern Taiwan Strait sands (East Asia) [J]. Marine Geology, 2021, 436: 106495.*

<https://doi.org/10.1016/j.margeo.2021.106495>

**摘要:** 台湾海峡是连接东亚地区东海和南海的纽带。海峡两岸复杂的海洋动力学、巨量的沉积物输入以及不同的构造、气候和基岩岩性背景,使其成为研究沉积物源-汇系统的理想场所。虽然海峡的泥质沉积物已经得到了很好的研究,但砂质的组成和物源仍未得到充分的研究。本文通过对台湾海峡南部及邻近代表性河流砂体的岩相和重矿物资料的分析,探讨了其物源和沉积机制。如预期的那样,中国东南部河砂以石英和长石为主,而台湾向西流动的山区河砂则富含岩屑和重变质矿物。台湾海峡南部砂体骨架颗粒和重矿物的组成和结构存在明显的空间变化。格架颗粒物源模拟结果表明,台湾海峡西南缘(水深 30~60 m)砂体主要由华南东南缘河流供给。台湾河流对远离台湾岛(约 100-300 km)的台湾海峡中西部(40-60 m)和台湾浅滩南部(50 m 以下)贡献显著。台湾浅滩(20~30 m)砂体成分成熟度极高,以粗粒、圆形石英为主。这些砂体,以前被认为是残余沉积物,已经被现代高能水动力条件强烈地改变,也可以解释为再旋回沉积物。这些结果表明,现代河砂最终沉积在海峡较深水区,而不是浅水区(台湾浅滩)。沙粒的组成和分布与台湾海峡海底地形密切相关。结合以往的泥质带研究,我们认为在气候、洋流和海底地貌条件复杂的浅层大陆架上,砂与泥具有不同的命运。这项研究还强调了海峡中现代砂和以前的残余砂均具有重要性。我们的发现对更好地理解具有巨大河流沉积物输入和高波浪/潮汐能量的陆棚沉积体系具有重要意义。

**ABSTRACT:** The Taiwan Strait serves as a link between the East China Sea and South China Sea in East Asia. Complex ocean dynamics, huge sediment inputs and distinct tectonic, climatic and bedrock lithological settings of the two sides of the strait make it ideal for sediment source-to-sink studying. While mud sediments in the strait have been well investigated, sand composition and provenance remain understudied. Here, we present framework petrography and heavy mineral data of sands from the southern Taiwan Strait and the adjacent representative rivers to characterize sand

provenance and depositional mechanisms. As expected, the SE China river sands are dominated by quartz and feldspar, whereas sands from the westward-flowing mountainous rivers in Taiwan are rich in lithic fragments and heavy minerals of metamorphic origin. The southern Taiwan Strait sands show significant spatial variations in composition and texture of the framework grains and heavy minerals. Framework grain-based provenance modeling results show that sands in the southwest margin of Taiwan Strait (water depth of 30–60 m) are mainly supplied by SE China rivers. Taiwan mountainous rivers made prominent contributions to the central-western Taiwan Strait (40–60 m) and the south of Taiwan Shoal (below 50 m), both of which are far away from the Taiwan island (ca. 100–300 km away). Furthermore, sands from the Taiwan Shoal (20–30 m) show extremely high compositional maturity and are mainly composed of coarse, rounded quartz. These sands, previously proposed as relict sediments, have been intensely altered by modern high-energy hydrodynamic conditions and can also be interpreted as palimpsest sediments. These results demonstrate that modern river-derived sands are eventually deposited in relatively deep-water regions in the strait, rather than the shallow regions (Taiwan Shoal). We propose that the sand composition and distribution are closely related to the submarine topography of the Taiwan Strait. Combining previous mud belt investigations, we suggest that sands and muds tend to have different fates in shallow continental shelves with complex climate, ocean current and seafloor landform conditions. This study also highlights the importance of both modern and relict sands in the strait and our findings are important to better understanding of shelf sedimentary systems with huge river-sediment-input and high wave/tidal-current-energy.

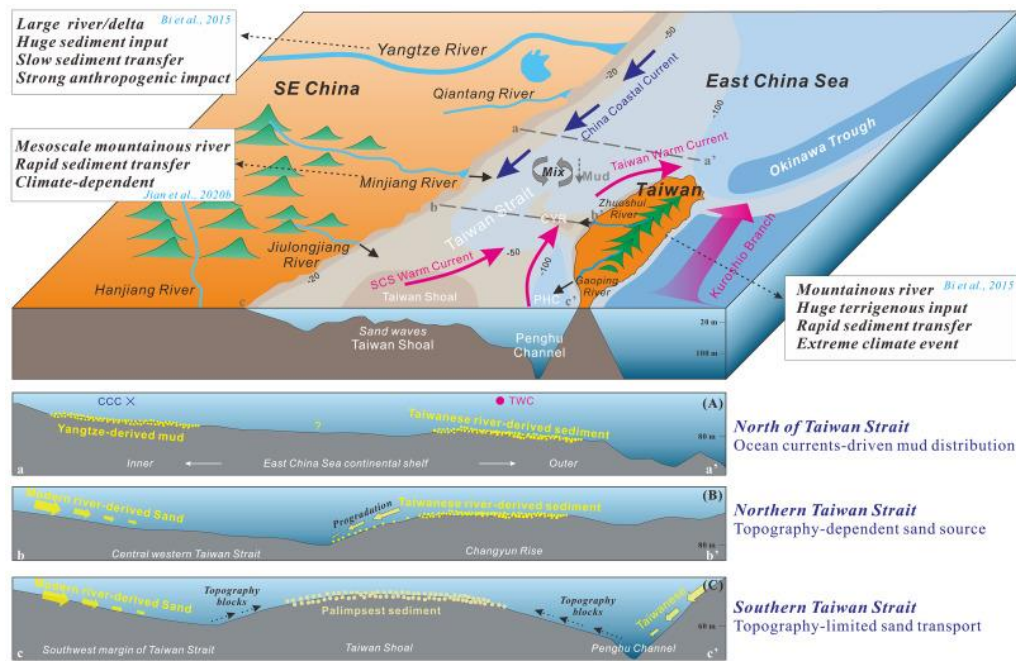


**Figure 1.** Schematic sediment source-to-sink model around the East China Sea continental shelf and the Taiwan Strait. Simplified submarine topography was outlined. For sediment source, three distinct types of sediment supply and transport systems develop in subtropical-tropical East Asia (Bi et al., 2015; Jian et al., 2020b). Drainage basin bedrock lithology and morphology, tectonic settings, climatic conditions, and anthropogenic activities determine the differences in sediment flux and composition among these areas. Ocean currents and seafloor topography subsequently dominate the fate of river-derived sediment deposited on continental shelf. Three profiles cross the ECS shelf and the Taiwan Strait was marked with grey dashed lines. Profile (a) is at the south ECS shelf to the north of the Taiwan Strait. Yangtze River-derived clays carried by southward China Coastal Current (CCC) deposited along the Zhejiang-Fujian coast, and sediments derived by Taiwanese rivers are carried northward by Taiwan Warm Current and deposit near northern Taiwan island in outer ECS shelf. Profile (b) covers the Changyun Rise (water depth of 30 m) and the central-western Taiwan Strait. Due to high yield and episodic events, Taiwanese fluvial sediments on the Changyun Rise progressively prograde westward and form subaqueous delta (Liu et al., 2008a). Profile (c) indicates that topography contributes a major impact of sands distribution in the southern Taiwan Strait. The discharged sands of modern SE China rivers and Taiwanese rivers deposit in coastal region and are blocked by shallow submarine topography of the Taiwan Shoal. With less modern rivers-derived sediment, relict sediments are preserved in the Taiwan Shoal and experienced intensely alteration by high-energy hydrodynamic conditions.

### 3. 中国东南仙云洞在 Heinrich 4 期间记录的东亚夏季风的三阶段结构

翻译人: 杨会会 11849590@mail.sustech.edu.cn



Zhang X, Qiu W Y, Jiang X Y, et al., *Three-phase structure of the East Asia summer monsoon during Heinrich Stadial 4 recorded in Xianyun Cave, southeastern China [J]. Quaternary Science Reviews, 2021, 274, 107267*

<https://doi.org/10.1016/j.quascirev.2021.107267>

**摘要:** Heinrich 4 (HS4)是格陵兰冰芯记录的 6 次事件中规模最大的一次, 发生于 40-38.2ka BP。然而, 它的结构、驱动因素和相关的全球水文气候变化仍然知之甚少。本文利用中国东南部仙云洞 8 年分辨率的石笋  $\delta^{18}\text{O}$  记录重建了 41.33-37.04 ka BP 之间东亚夏季风(EASM)百年-千年尺度的变化。仙云洞记录在 HS4 期间 40.04-37.76 ka BP 显示出相应的弱季风期, 是亚洲季风区第一个明确揭示东亚夏季风三阶段结构的直接证据。第一阶段为减弱的季风期 (40.04-39.54 ka BP), 伴随着热带辐合带(ITCZ)的南移。第二阶段是一个长期的弱季风期, 从 39.54-28.48 ka 跨越了 1.6 ka, 对应北大西洋冰筏碎屑沉积事件和巴西东北部的强降雨时期, 这表明在这段时间内, ITCZ 在它的最南端徘徊。该阶段结束后, EASM 在逐渐增强直到 37.76 kyr BP, 持续了 720 年。仙云洞记录的特征与格陵兰北部伊姆斯冰芯钻孔(NEEM) $^{17}\text{O}$ -excess 指标所记录的低纬气候信号一致, 与巴西东北部石笋记录的干湿转变反相一致。这些关系表明热带大气/海洋环流对北半球高纬度驱动的多阶段响应。我们的发现为理解低纬度和高纬度气候遥相关以及季风和热带水文循环之间的关系提供了重要的证据。

**ABSTRACT:** The Heinrich Stadial (HS) 4 event was the largest of the six HS events and occurred from 40.0 to 38.2 kyr BP (thousand years before present, where present = 1950 CE) recorded in Greenland ice cores. However, its structure, forcings, and related global hydroclimate variation remain poorly understood. Here, an 8-yr resolved stalagmite  $\delta^{18}\text{O}$  record from Xianyun Cave, southeastern China, is used to reconstruct the multidecadal-to-millennial-scale changes of the East Asian summer monsoon (EASM) from  $41.33 \pm 0.09$  to  $37.04 \pm 0.05$  kyr BP. The Xianyun record shows a corresponding weak monsoon interval from  $40.04 \pm 0.07$  to  $37.76 \pm 0.05$  kyr BP during HS

4 and is the first direct evidence in the Asian monsoon realm to clearly reveal a three-phase EASM structure. The first phase began with a weakening monsoon from  $40.04 \pm 0.07$  to  $39.54 \pm 0.06$  kyr BP, associated with a southward shift of the Intertropical Convergence Zone (ITCZ). The second phase was a long weak monsoon, spanning 1.06 kyr from  $39.54 \pm 0.06$  to  $38.48 \pm 0.05$  kyr BP and corresponding to an ice-rafted debris event in the North Atlantic Ocean and an intense pluvial phase in Northeast (NE) Brazil, suggesting that the ITCZ lingered at its southernmost position during this interval. Following the end of this phase, EASM was gradually enhanced for 720 yrs through  $37.76 \pm 0.05$  kyr BP. The feature expressed in the Xianyun record agrees with the variations in low-latitude climate signals recorded in the Northern Greenland Eemian Ice Drilling (NEEM)  $^{17}\text{O}$ -excess and anti-phase matches with dry-wet transition recorded in NE Brazilian stalagmites. These relations suggest multi-phased responses of tropical atmospheric/oceanic circulations to forcing from northern hemisphere high latitudes. Our findings offer essential evidence for understanding low- and high-latitude climate teleconnections and the relationship between the monsoon and the tropical hydrologic cycle.

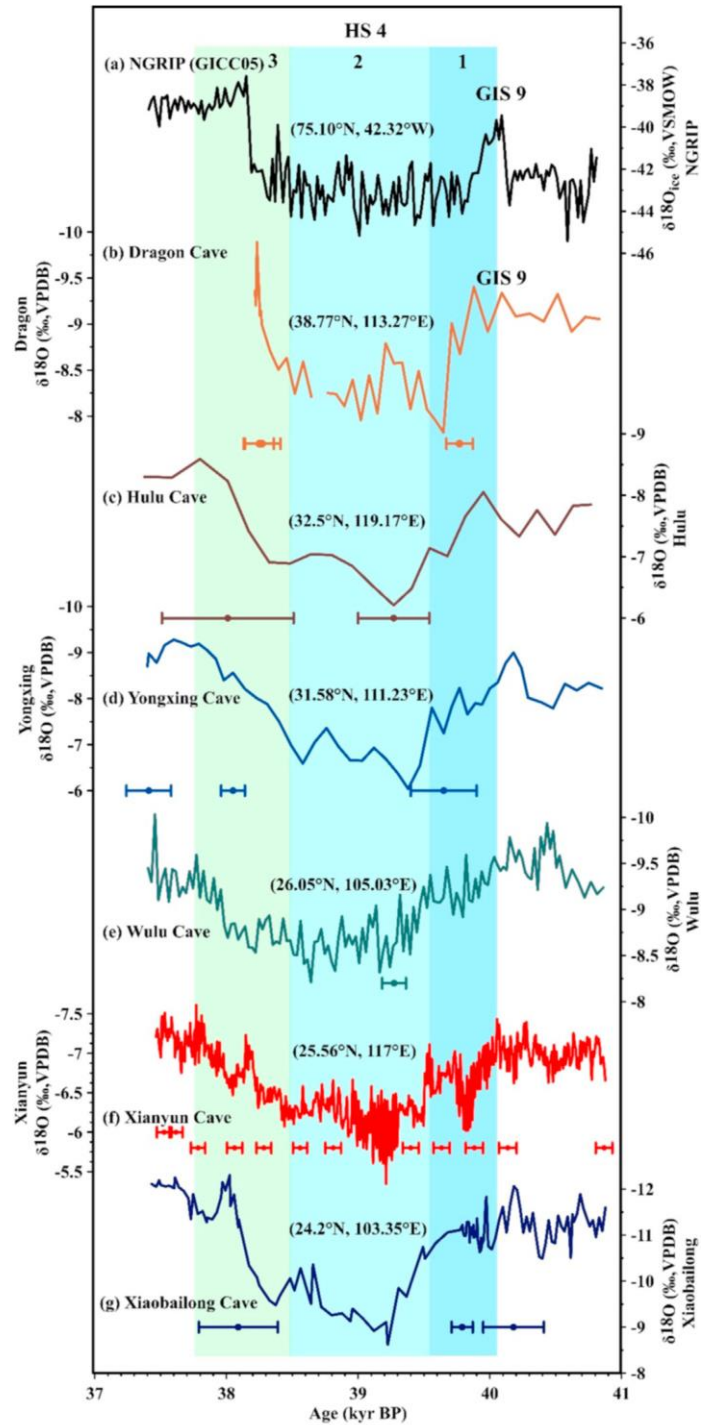


**Figure 1.** (a) Comparison of  $\delta^{18}\text{O}$  records between (a)  $\delta^{18}\text{O}$  ice of NGRIP record on GICC05 timescales (Svensson et al., 2008) and Chinese stalagmite records of (b) Dragon Cave (Dong et al., 2018), (c) Hulu Cave (Wang et al., 2001), (d) Yongxing Cave (Chen et al., 2016), (e) Wulu Cave (Liu et al., 2018), (f) Xianyun Cave (this study), and (g) Xiaobailong Cave (Cai et al., 2006). All records are plotted with their own age models.  $^{230}\text{Th}$  ages with error bars are color-coded by stalagmite records. Durations of phase 1, 2, and 3 of HS 4, based on Xianyun record are highlighted by vertical bars with colors of sky blue, ice

blue, and mint green, respectively. GIS 9 marks Greenland interstadial 9 interval. (For interpretation of the references to color in this figure legend, the reader is referred to the Web version of this article.)

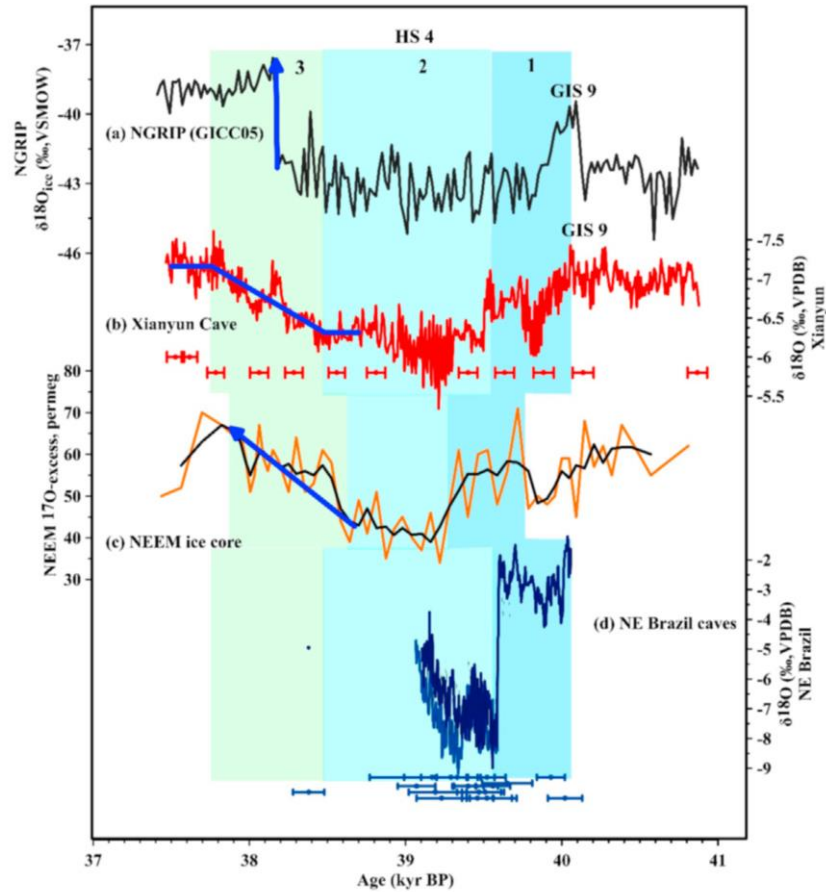


**Figure 2.** Comparison of records between (a)  $\delta^{18}\text{O}$  ice of the NGRIP record on GICC05 timescales (Svensson et al., 2008); (b)  $\delta^{18}\text{O}$  of Xianyun Cave (this study); (c)  $^{17}\text{O}$ -excess of NEEM ice core on GICC05 timescales (Guillevic et al., 2014); (d)  $\delta^{18}\text{O}$  of NE Brazil caves (Wendt et al., 2019). All records are plotted with their own age models.  $^{230}\text{Th}$  ages with error bars are color-coded by stalagmite records. Durations of phase 1, 2, and 3 of HS 4, based on Xianyun record are highlighted by vertical bars with colors of sky blue, ice blue, and mint green, respectively. GIS 9 marks Greenland interstadial 9 interval. (For interpretation of the color references in this figure legend, the reader is referred to the Web version of this article).

## 4. 地球构造碳输送带的演化

翻译人：曹伟 11930854@qq.com



Müller D, Mather B, Dutkiewicz A, et al. *Evolution of Earth's tectonic carbon conveyor belt* [J]. *Nature*, 2022, 605:629-639.

<https://doi.org/10.1038/s41586-022-04420-x>

**摘要：**在海洋深处隐藏着一条由板块构造推动的碳输送带。我们对其现代运作的理解是基于直接的观察，但其随时间的变化一直没有被量化。本文利用热力学模型重建大洋板块碳储层，追踪俯冲碳的去向。在 2.5 亿至 6600 万年前的中生代，板块构造过程在推动气候变化方面发挥了关键作用。三叠纪侏罗纪时期的变冷与固体地球气体排放的减少有关，而白垩纪时期的温室条件可能与高速板块构造驱动的气体排放翻倍有关。相关的碳俯冲超量进入次大陆地幔可能引发了北美钻石的形成。在新生代，大陆碰撞减缓了海底扩张，减少了构造驱动的排放，而深海碳酸盐沉积物成为地球上最大的碳汇。火山弧下的储层俯冲和挥发作用导致新生代碳排放增加，超过 2000 万年前的大洋中脊，成为碳排放的主要来源。新生代变冷期间固体地球碳排放量的增加需要大陆硅酸盐风化通量的增加来降低大气中的二氧化碳，这挑战了以前的观点，并为未来的碳循环模型提供了边界条件。

**ABSTRACT:** Concealed deep beneath the oceans is a carbon conveyor belt, propelled by plate tectonics. Our understanding of its modern functioning is underpinned by direct observations, but its variability through time has been poorly quantified. Here we reconstruct oceanic plate carbon reservoirs and track the fate of subducted carbon using thermodynamic modelling. In the Mesozoic era, 250 to 66 million years ago, plate tectonic processes had a pivotal role in driving climate change. Triassic Jurassic period cooling correlates with a reduction in solid Earth outgassing, whereas Cretaceous period greenhouse conditions can be linked to a doubling in outgassing, driven by high-speed plate tectonics. The associated carbon subduction superflux into the subcontinental mantle may have sparked North American diamond formation. In the Cenozoic era, continental collisions slowed seafloor spreading, reducing tectonically driven outgassing, while deep-sea carbonate sediments emerged as the Earth's largest carbon sink. Subduction and devolatilization of this

reservoir beneath volcanic arcs led to a Cenozoic increase in carbon outgassing, surpassing mid-ocean ridges as the dominant source of carbon emissions 20 million years ago. An increase in solid Earth carbon emissions during Cenozoic cooling requires an increase in continental silicate weathering flux to draw down atmospheric carbon dioxide, challenging previous views and providing boundary conditions for future carbon cycle models.

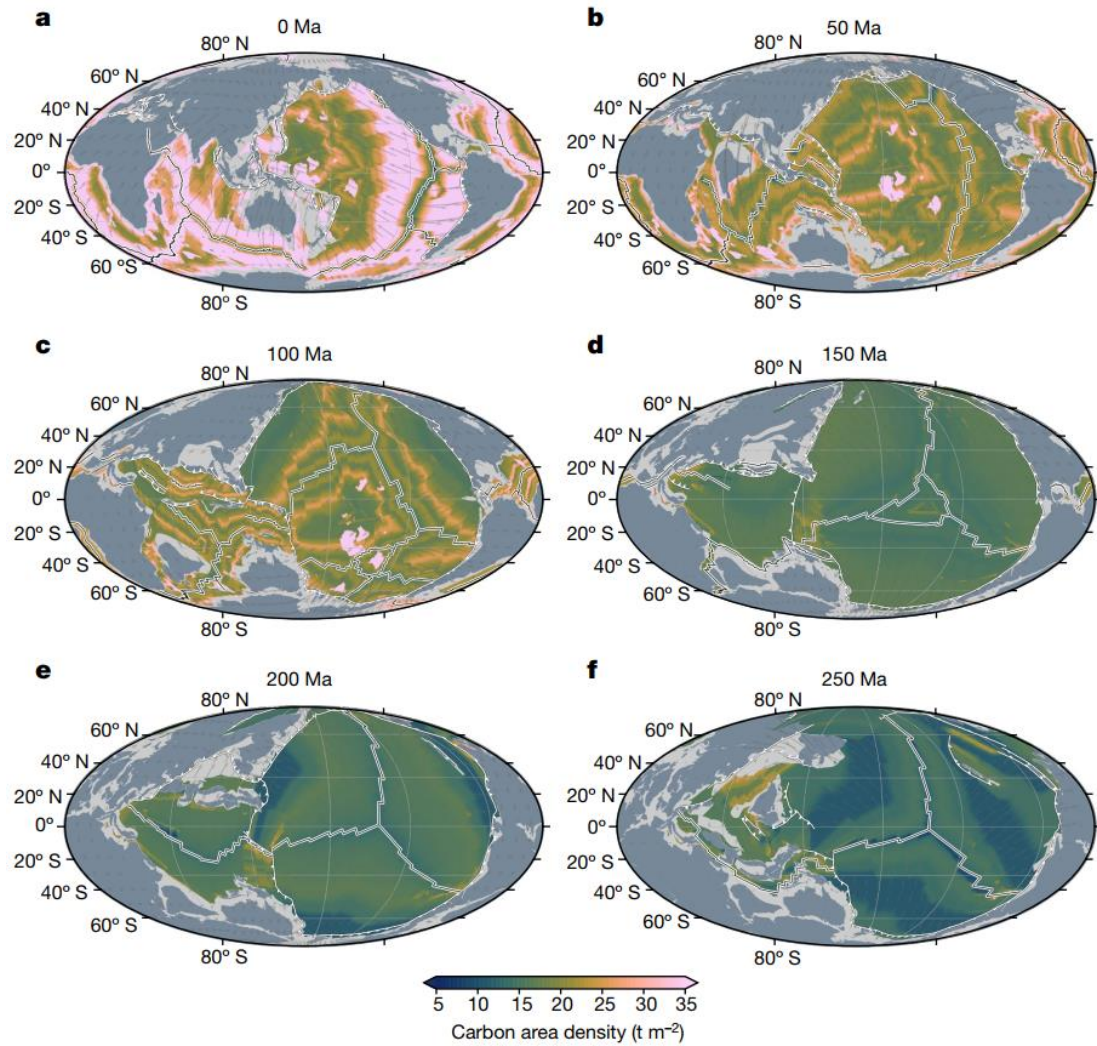


**Figure 1.** Carbon area density in the oceanic lithosphere through time.

## 5. 马里亚纳海沟沉积物中的磁性有孔虫特征



翻译人：王敦繁 Dunfan-w@foxmail.com

Yang, H., Peng, X., Gooday, A.J., et al. *Magnetic foraminifera thrive in the Mariana Trench. *Geochem [J]. Geochemical Perspectives Letters*, 2022; 21, 23–27.*

<https://doi.org/10.7185/geochemlet.2212>

**摘要：**单细胞磁性微生物包括趋磁细菌和一些原生生物。虽然细菌(原核生物)中的磁性小体磁铁矿已经得到了很好的研究，但关于原生生物(真核生物)中磁性矿物的特征和来源却知之甚少。来自马里亚纳海沟(6980-10911 米深)的有孔虫 *R. bilocularis* 体内含有磁铁矿晶体。因此，这种物种可以根据磁场定向。这种磁铁矿在化学和物理上与周围沉积物中的具有明显区别。这些磁性矿物与细菌磁小体的不同之处在于：大小多变、多孔结构、非链式排列、包裹在脂质膜中。综合现有证据，表明磁铁矿是生物成因，尽管不能排除沉积成因。这是深渊深处磁原生生物的第一个记录，为地球极端环境下的生物磁学打开了一个新的窗口。

**ABSTRACT:** Unicellular magnetic microorganisms include magnetotactic bacteria and some protist species. Although magnetosome magnetite in bacteria (prokaryotes) is well studied, little is known regarding the characteristics and origin of magnetic minerals in protists (eukaryotes). Stercomata stored within tests of the hadal foraminifera *R. bilocularis* from the Mariana Trench (6980–10,911 m depth), contain magnetite crystals. As a result, this species can orient in accordance with magnetic fields. The magnetite differs chemically and physically from that in the surrounding sediments. The crystals also differ from bacterial magnetosomes in being of variable size, porous structure, not arranged in chains, and encapsulated in a lipid membrane. Putting available evidence together indicates a biological origin of the magnetite, although a sedimentary source cannot be eliminated. This is the first record of a magnetic protist from hadal depths, opening a new window for the biomagnetism in the Earth's extreme environment.

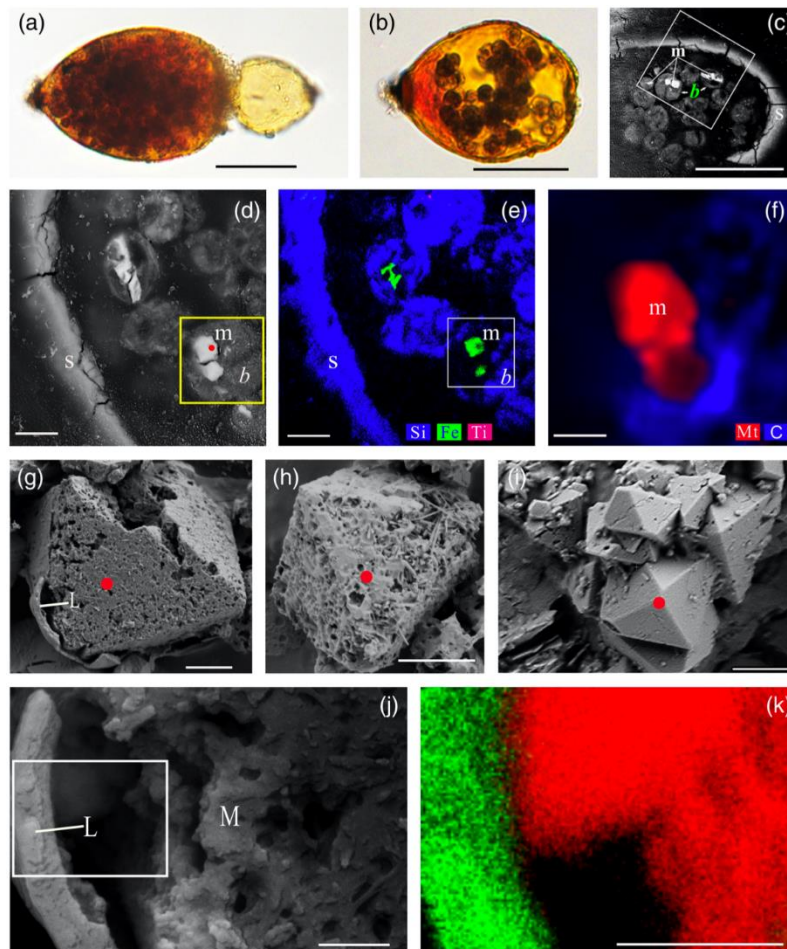


**Figure 1.** Magnetite in the foraminifera *R. bilocularis*. (a) LM (light microscopy) image showing the rusty colour of the organic walled test of *R. bilocularis*. (b) LM image of the larger chamber of *R. bilocularis* stained with Rose Bengal, with fresh stercomata (waste pellets) and stained cytoplasm concentrated just inside the aperture. (c) SEM image of a thin section of *R. bilocularis* from the Challenger Deep with numerous stercomata (b) inside the test (s). Magnetite (m) is contained in the stercomata. (d) Enlarged SEM image of the area indicated by the white rectangle in (c). Magnetite (m) is contained in the stercomata (b), within the yellow box. Raman analysis position is marked with a red dot. (e) NanoSIMS elemental mapping of *R. bilocularis*. Blue = Si; Green = Fe; Red = Ti. SEM-EDX elemental maps are presented in Figure S-15. (f) Raman spectral combined images obtained from a stercome containing magnetite, indicating magnetite and organic carbon in stercomata, respectively. (g, h, i) Secondary electron image of magnetite extracted from *R. bilocularis* showing a euhedral and porous structure. L = carbon-containing membrane. (j) An enlarged SEM image of the carbon-containing membrane enveloping the magnetite. L = carbon-containing membrane, M = magnetite. (k) The elemental mapping of the area in white rectangular.

## 6. 菲律宾海中部深海沉积物第四纪的磁性地层学和区域沉积动力学



翻译人：王浩森 11930841@mail.sustech.edu.cn

Yi L, Hu B, Zhao J, et al. *Magnetostratigraphy of abyssal deposits in the Central Philippine Sea and regional sedimentary dynamics during the Quaternary*[J]. *Paleoceanography and Paleoclimatology*, 2022: e2021PA004365.

<https://doi.org/10.1029/2021PA004365>

**摘要：**菲律宾海位于西太平洋暖池内，是一个典型的风尘后沉积区域。在这里，我们利用古地磁地层学和菲律宾海中部第四纪深海沉积物的粒度分布来研究控制区域沉积和古环境变化的因素。我们的主要结果如下：(a)建立了菲律宾海中部第四纪沉积物的可靠年代学框架。

(b) 区域沉积中心在中更新世向东扩展。(c) 深海沉积物的平均粒径为 7–8  $\mu\text{m}$ ，不同地点之间的差异较小。将地质年代学框架与中更新世过渡期的各种古环境事件进行比较表明，沉积过程可能与亚洲内陆到热带太平洋地区的全球气候的重大转变相关，而风成沉积的变化可能是主要的原因。根据沉积动力学粒度指标及其与各种古环境指标的比较表明，研究区域的风成输入、海洋环流和热带太平洋地带 SST 梯度的相对贡献率分别约为 23%、9%和 68%。热过程在深海沉积动力学中的重要性表明，从气象到地质时间尺度，菲律宾海中部最深部分 (>5000 m) 的区域上升流和独特的海底地形可能会对上层海洋 (亚) 中尺度涡旋产生长期影响。

**ABSTRACT:** The Philippine Sea is a typical region of aeolian dust reposition and is located within the Western Pacific Warm Pool. Here, we use the paleomagnetic stratigraphy and the grain-size distributions of Quaternary abyssal deposits in the Central Philippine Sea to investigate the factors controlling regional sedimentary and paleoenvironmental changes. Our principal results are as follows: (a) A reliable geochronologic framework for Quaternary sediments in the Central Philippine Sea is established. (b) An eastward expansion of the regional depocenter in the Middle Pleistocene is observed. (c) The mean grain size of the abyssal sediments is 7–8  $\mu\text{m}$ , and there are only minor differences between the sites. Comparison of the geochronological framework with

various paleoenvironmental events during the Mid-Pleistocene Transition shows that sedimentary processes can be correlated to a major transition in global climate which affected regions from the Asian interior to the tropical Pacific, and that changes in aeolian sedimentation are likely the predominant factor responsible. A derived grain-size proxy of the sedimentary dynamics and its comparison with various paleoenvironmental proxies show that the relative contributions are roughly estimated as 23%, 9%, and 68% for aeolian inputs, oceanic circulation, and the tropical Pacific zonal SST gradient, respectively, in the studied region. The relative importance of tropical processes in abyssal sedimentary dynamics highlights the possibility of the long-term influence of (sub)mesoscale eddies in the upper ocean, via regional upwelling and unique submarine topography, on the deepest part (>5,000 m) of the Central Philippine Sea, from meteorological to geological timescales.

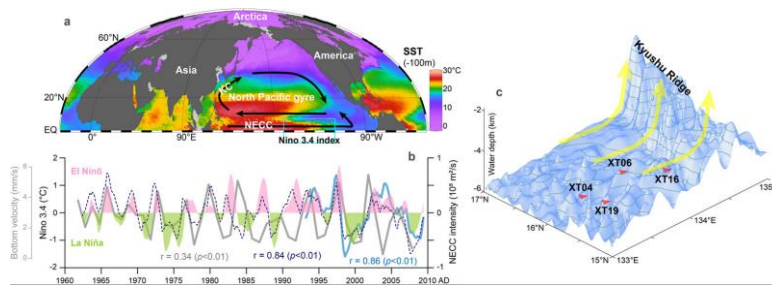


**Figure 1.** A mechanism explaining the linkage between regional sedimentary dynamics in the Central Philippine Sea (PGSI) and El Niño-Southern Oscillation (ENSO)-like changes. (a) sea surface temperature (SST) distribution across the North Pacific. NECC, North Equatorial Countercurrent; KC, Kuroshio Current. The circulation patterns are modified from You (2003) and Keeling et al. (2010). The data are from the World Ocean Atlas 2013 (WOA2013) (Garcia et al., 2013; Levitus et al., 2014). (b) Comparison of NECC intensity (bold line, from OSCAR data; dashed line, simulated by a linear Rossby wave model) and the Nino 3.4 index anomaly (Zhao et al., 2013). Gray line, annual bottom-water velocity in a region of [133.0°–134.5°E, 15.5°–16.5°N] at 5,000 m water depth (this study), from the Simple Ocean Data Assimilation (SODA version 2.2.4), which is an ocean reanalysis data set (Carton & Giese, 2008; Carton et al., 2000; National Center for Atmospheric Research Staff, 2016), consisting of gridded variables for the global ocean. (c) Location of sites with grain-size records and an upwelling-induced top-to-bottom linkage.

## 7. 泥盆纪是持续非均变古地磁场?



翻译人: 张伟杰 12031188@mail.sustech.edu.cn

van der Boon A, Biggin A J, Thallner D, et al. *A persistent non-uniformitarian paleomagnetic field in the Devonian?* [J]. *Earth-Science Reviews*, 2022: 104073.

<https://doi.org/10.1016/j.earscirev.2022.104073>

**摘要:** 泥盆纪长期以来一直是古地磁学难以研究的一个时期。泥盆纪古地磁数据通常难以解释, 并且沉积和火成岩都普遍存在复杂的部分或全部重磁化。因此, 利用视极移曲线进行板块构造运动的重建具有很大的不确定性。同样泥盆纪地磁极性年表的约束性也较差。对火成地层的古强度研究表明, 当时磁场比现代磁场弱得多, 并且有假设认为当时存在多次极性倒转事件。我们对德国、波兰和加拿大的中上泥盆统剖面进行了采样, 这些剖面显示牙形石蚀变指数较低, 表明热成熟度较低。虽然没有明显的加热或再矿化引起的重磁化, 但是结果表明这些数据存在明显问题。我们将我们的数据与其他泥盆系的磁地层研究进行了比较, 并回顾了地质时间尺度上呈现的极性模式。结合古强度结果, 我们认为泥盆纪时期的磁场可能非常弱, 而且部分是非偶极磁场, 因此从泥盆纪岩石中获得可靠的原生古地磁数据是具有挑战性的。仔细检查所有这些特别的数据, 是推动我们了解泥盆纪磁场的最佳方式。古强度研究表明, 泥盆纪的古磁场强度与埃迪卡拉纪相似。泥盆纪-石炭纪边界附近的异常孢子提供的独立证据表明: 与 Hangenberg 事件有关的陆生物种灭绝是由 UV-B 辐射增加引起的, 这支持了弱地场假说。在泥盆纪时期, 一个弱的、可能非偶极磁场可能部分是由于真极移产生的, 并且使赤道地区的核-幔热流最大化。它也可能影响了这一时期的进化和灭绝。在泥盆纪有大量的古生物危机, 我们提出一个问题, 地球磁场是否影响了这些危机?

**ABSTRACT:** The Devonian has long been a problematic period for paleomagnetism. Devonian paleomagnetic data are generally difficult to interpret and have complex partial or full overprints—problems that arise in data obtained from both sedimentary and igneous rocks. As a result, the reconstruction of tectonic plate motions, largely performed using apparent polar wander paths, has large uncertainty. Similarly, the Devonian geomagnetic polarity time scale is very poorly constrained. Paleointensity studies from volcanic units suggest that the field was much weaker than

the modern field, and it has been hypothesised that this was accompanied by many polarity reversals (a hyperreversing field). We sampled Middle to Upper Devonian sections in Germany, Poland and Canada which show low conodont alteration indices, implying low thermal maturity. We show that there are significant issues with these data, which are not straightforward to interpret, even though no significant heating or remineralisation appears to have caused overprinting. We compare our data to other magnetostratigraphic studies from the Devonian and review the polarity pattern as presented in the Geologic Time Scale. Combined with estimates for the strength of the magnetic field, we suggest that the field during the Devonian might have been so weak, and in part non-dipolar, that obtaining reliable primary paleomagnetic data from Devonian rocks is challenging. Careful examination of all data, no matter how unusual, is the best way to push forward our understanding of the Devonian magnetic field. Paleointensity studies show that the field during the Devonian had a similar low strength to the Ediacaran. Independent evidence from malformed spores around the Devonian-Carboniferous boundary suggests that the terrestrial extinction connected to the Hangenberg event was caused by increased UV-B radiation, supporting the weak field hypothesis. A fundamentally weak and possibly non-dipolar field during the Devonian could have been produced, in part, by true polar wander acting to maximise core-mantle heat flow in the equatorial region. It may also have influenced evolution and extinctions in this time period. There are a large number of paleobiological crises in the Devonian, and we pose the question, did the Earth's magnetic field influence these crises?

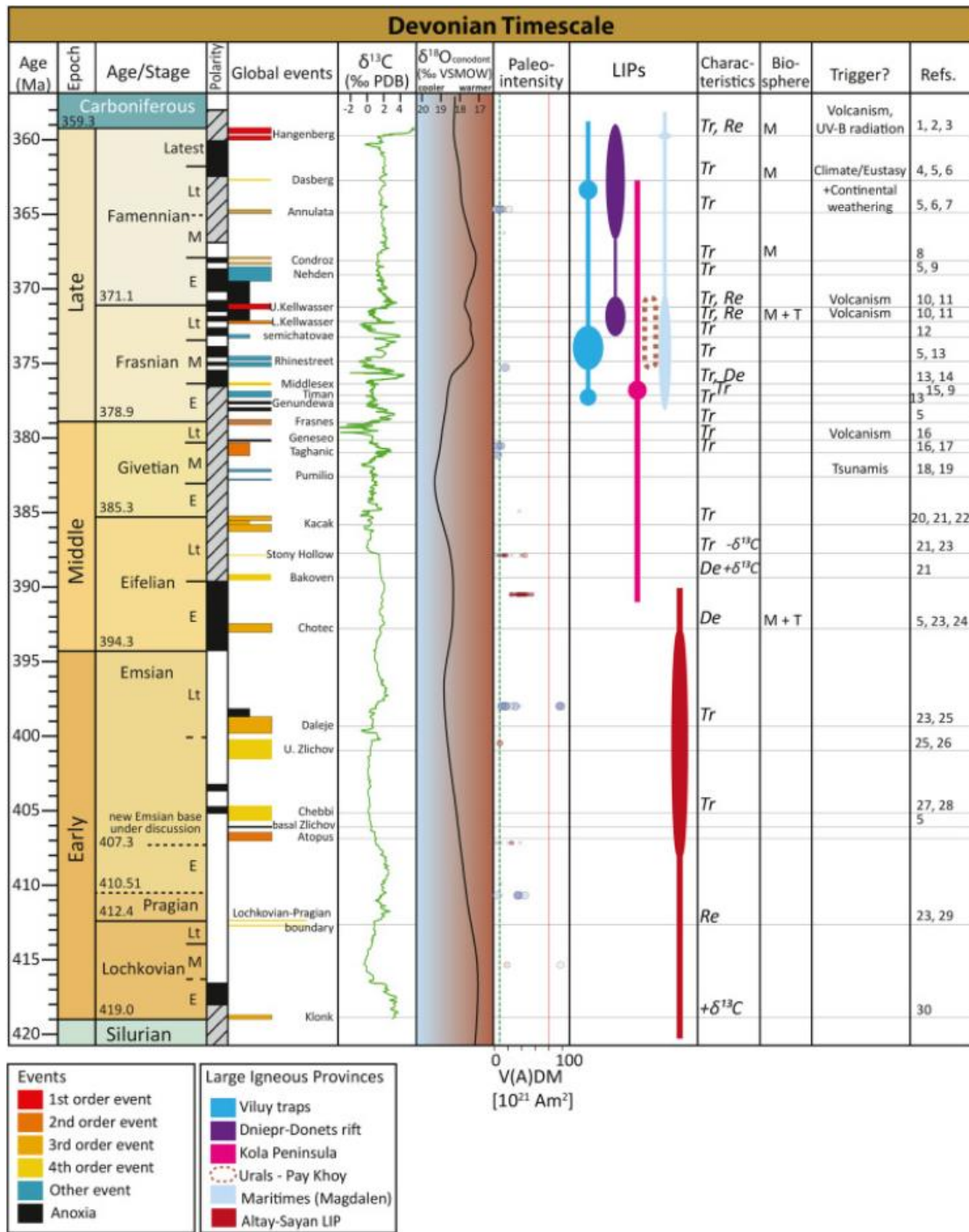


**Figure 1.** Overview of biotic events and crises in the Devonian. Timescale from GTS2020 (Becker et al., 2020), magnetic polarity in black (white) is normal (reversed), grey is unknown. Global events from Becker et al. (2020, 2016),  $\delta^{13}\text{C}$  is in reference to the Pee Dee Belemnite (PDB),  $\delta^{18}\text{O}$  is in reference to the Vienna Mean Standard Ocean Water (VSMOW). Paleointensities from the PINT database (Bono et al., 2022) and Shcherbakova et al. (2021), green (red) line is the field strength in the Ediacaran (present day), large igneous provinces (LIPs) are after Racki (2020) and Ernst et al.,

2021, Ernst et al., 2020. Characteristics: Tr = transgression, Re = regression, De = deepening event,  $-\delta^{13}\text{C}$  = negative  $\delta^{13}\text{C}$  excursion,  $+\delta^{13}\text{C}$  = positive  $\delta^{13}\text{C}$  excursion. Part of biosphere affected: M = marine, T = terrestrial. To scale the volcanic pulses to the timescale of Becker et al. (2020), we used the Devonian-Carboniferous boundary, Frasnian-Famennian and Givetian-Frasnian boundaries in the fig. of Racki (2020). References : 1 - Kaiser et al. (2016), 2 - Piszczowska et al. (2020), 3 - Marshall et al. (2020), 4 - Hartenfels and Becker (2009), 5 - House (2002), 6 - Hartenfels and Becker (2016), 7 - Percival et al. (2019), 8 - Becker et al. (2016), 9 - Becker and House (1997), 10 - Racki et al. (2018), 11 - Carmichael et al. (2019), 12 - Ziegler and Sandberg (1997), 13 - House and Kirchgasser (1993), 14 - Sandberg et al. (2002), 15 - Racki et al. (2004), 16 - Brett et al. (2011), 17 - Aboussalam and Becker (2011), 18 - Lottmann (1990), 19 - Becker and Aboussalam (2004), 20 - Königshof et al. (2016), 21 - DeSantis and Brett (2011), 22 - Suttner et al. (2021), 23 - Walliser (1996), 24 - Brocke et al. (2016), 25 - Tonarová et al. (2017), 26 - García-Alcalde (1997), 27 - Becker et al. (2020), 28 - Becker and Aboussalam (2011), 29 - Chlupáč and Kukul (1988), 30 - Małkowski and Racki (2009).

## 8. 伊比利亚半岛全新世人类活动对火灾的影响



翻译人: 李海 12031330@mail.sustech.edu.cn

*Sweeney L, Harrison S P, & Vander M. Assessing anthropogenic influence on fire history during the Holocene in the Iberian Peninsula [J]. Quaternary Science Reviews, 2022, 287, 107562.*

<https://doi.org/10.1016/j.quascirev.2022.107562>

**摘要:** 气候变化和人类活动对全新世区域火灾的影响的相对重要性仍然是一个有争议的问题。新石器时代农业的兴起为研究人类活动对火灾的影响提供了机会。在本研究中, 作者利用沉积炭记录重建了伊比利亚半岛 10000-3500 cal. BP 之间的火灾变化。作者基于考古材料的放射性碳年代比较了区域火灾历史和人口规模变化, 并将火灾记录和人口与考古数据显示的该区农业活动开始的时间进行了比较。伊比利亚总体上有两次人口快速增长的时间段, 分别集中在约 7400 cal. BP 和约 5400 cal. BP。整个地区或更局部的人口快速增长时期与木炭沉积的变化不密切相关。大约在新石器时代开始前 400 年, 木炭的沉积就已经开始增加, 并在此后约 750 年继续增加, 表明火的变化与农业的兴起没有直接的关系。同时, 木炭沉积的变化与后期人口快速增长期之间没有直接关系。在整个分析期间, 人口规模和木炭沉积之间也没有显著关系。研究结果表明, 农业的兴起和随后的人口增长与伊比利亚半岛的火灾变化没有直接关系, 支持了火灾变化主要受气候等其他因素驱动的观点。

**ABSTRACT:** The relative importance of climate change and human activities in influencing regional fire regimes during the Holocene is still a matter of debate. The introduction of agriculture during the Neolithic provides an opportunity to examine the impact of human activities on fire regimes. Here, we examine changes in fire regimes across Iberia between 10,000 and 3500 cal. BP, reconstructed using sedimentary charcoal records. We compare the regional fire history with estimates of changes in population size, reconstructed based on summed probability distributions of radiocarbon dates on archaeological material. We also compare the fire records and population reconstructions with the timing of the onset of agriculture across the region as indicated by archaeological data. For Iberia as a whole, there are two intervals of rapid population increase centred on ca. 7400 and ca. 5400 cal. BP. Periods of rapid population growth, either for the region

as a whole or more locally, do not closely align with changes in charcoal accumulation. Charcoal accumulation had already begun to increase ca. 400 years prior to the onset of the Neolithic and continued to increase for ca. 750 years afterwards, indicating that changes in fire are not directly associated with the introduction of agriculture. Similarly, there is no direct relationship between changes in charcoal accumulation and later intervals of rapid population growth. There is also no significant relationship between population size and charcoal accumulation across the period of analysis. Our analyses show that the introduction of agriculture and subsequent increases in population are not directly linked with changes in fire regimes in Iberia and support the idea that changes in fire are largely driven by other factors such as climate.

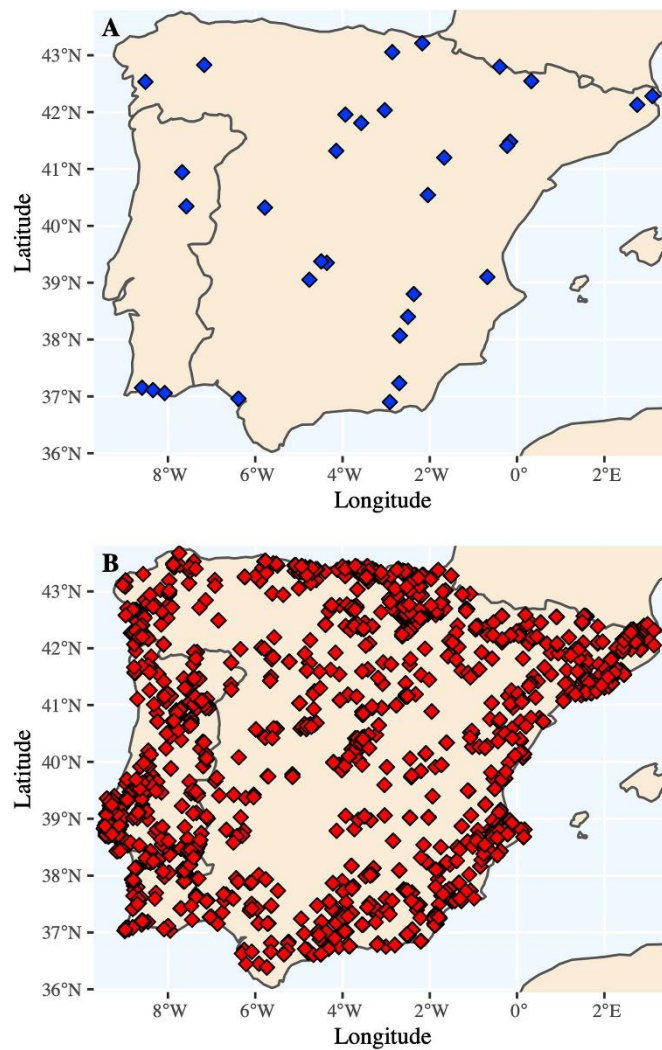


**Figure 1.** Maps of Iberia showing the locations of the charcoal (A) and archaeological (B) sites.

## 9. 相对海平面变化数据指示晚全新世 Pine Island Bay 并没有发生明显的冰盖变化



翻译人：张亚南 zhangyn3@mail.sustech.edu.cn

Braddock S, Hall B L, Johnson, J S, et al. *Relative sea-level data preclude major late Holocene ice-mass change in Pine Island Bay [J]. Nature Geoscience, 2022.*

<https://doi.org/10.1038/s41561-022-00961-y>

**摘要：** Thwaites 和 Pine Island 冰盖的快速消减共同决定了现今南极西部冰盖的冰量损失，并与失控的冰消期场景相关。了解这些冰川是否在中全新世大幅减少，随后恢复到现在的水平，其对于评估当前冰川消减是否不可逆转具有重要意义。文中，作者通过放射性碳年龄重建了冰川附近海滩的相对海平面变化，能够检测阿蒙森海区域不同冰负荷状态下的变化。结果表明过去 5.5 ka 以来相对海平面平稳下降，没有出现冰盖大幅度变化所导致的急剧海平面变化。此外，目前基岩的抬升速率比长期海平面下降高一个数量级，表明区域地壳上覆冰盖负荷的减少，并暗示现在冰川的消退在过去 5.5 ka 中都是前所未有的。虽然不能排除接地线（grounding-line）的微小波动，但数据结果更容易解释为全新世早期的冰川消退，随后是到目前为止都相对稳定的冰川位置，这意味着 Thwaites 和 Pine Island 冰盖在过去 5.5 ka 并没有比现在大幅减少。

**ABSTRACT:** The rapidly retreating Thwaites and Pine Island glaciers together dominate present-day ice loss from the West Antarctic Ice Sheet and are implicated in runaway deglaciation scenarios. Knowledge of whether these glaciers were substantially smaller in the mid-Holocene and subsequently recovered to their present extents is important for assessing whether current ice recession is irreversible. Here we reconstruct relative sea-level change from radiocarbon-dated raised beaches at sites immediately seawards of these glaciers, allowing us to examine the response of the earth to loading and unloading of ice in the Amundsen Sea region. We find that relative sea level fell steadily over the past 5.5 kyr without rate changes that would characterize large-scale ice re-expansion. Moreover, current bedrock uplift rates are an order of magnitude greater than the rate

of long-term relative sea-level fall, suggesting a change in regional crustal unloading and implying that the present deglaciation may be unprecedented in the past ~5.5 kyr. While we cannot preclude minor grounding-line fluctuations, our data are explained most easily by early Holocene deglaciation followed by relatively stable ice positions until recent times and imply that Thwaites and Pine Island glaciers have not been substantially smaller than present during the past 5.5 kyr.

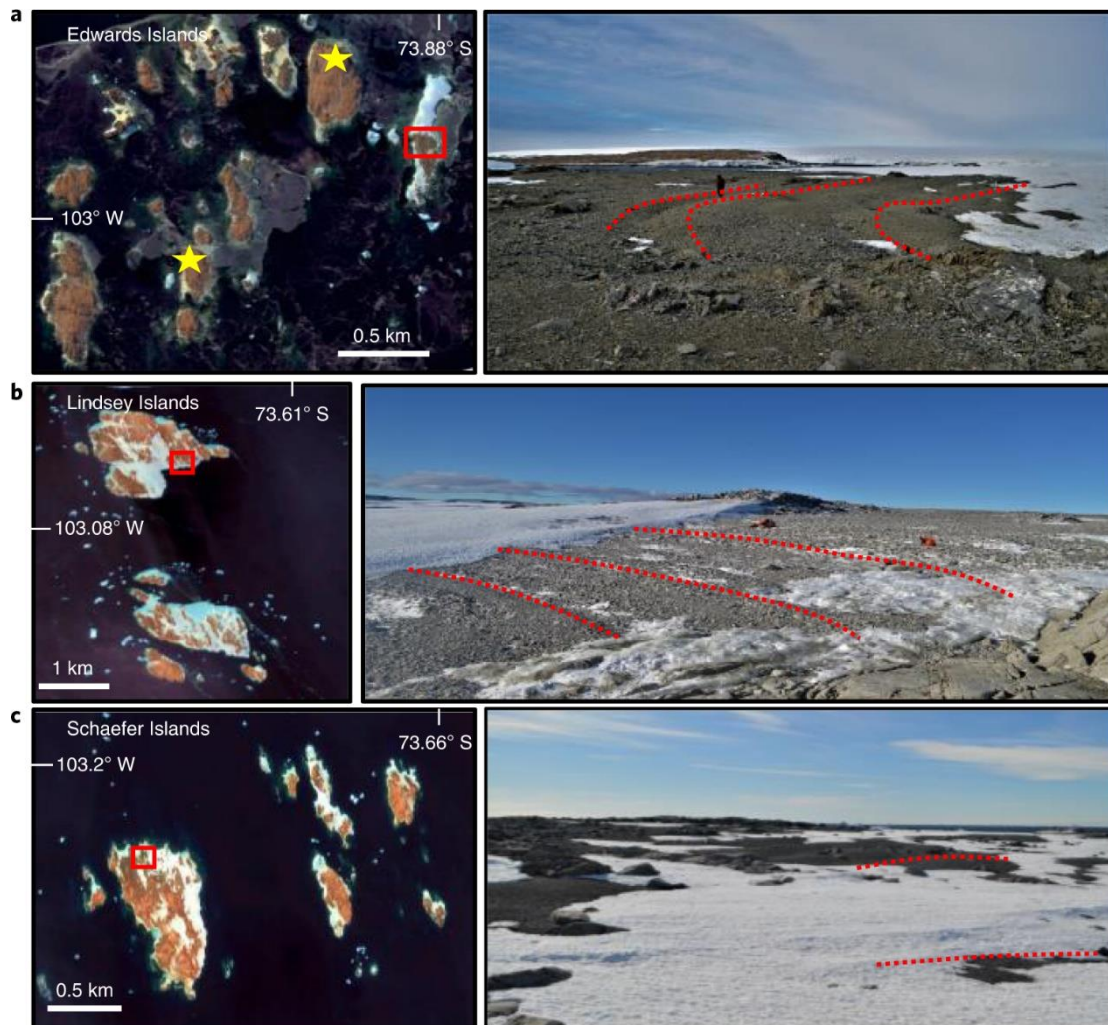


**Figure 1.** Satellite imagery and photographs of study sites in the Amundsen Sea Embayment. a–c, Left panel shows Edwards Islands (a), Lindsey Islands (b) and Schaefer Islands (c). Dashed lines in photos on right panels denote raised marine beaches from which shell and bone samples were collected. Photos are from sites corresponding to the red squares in adjacent imagery. Yellow stars in a denote location of additional sampled islands (Photos provided in Supplementary Figs. 2, 3 and 6). Credit: a–c (left), WorldView-2/DigitalGlobe, a Maxar Company; a–c (right), Scott Braddock.

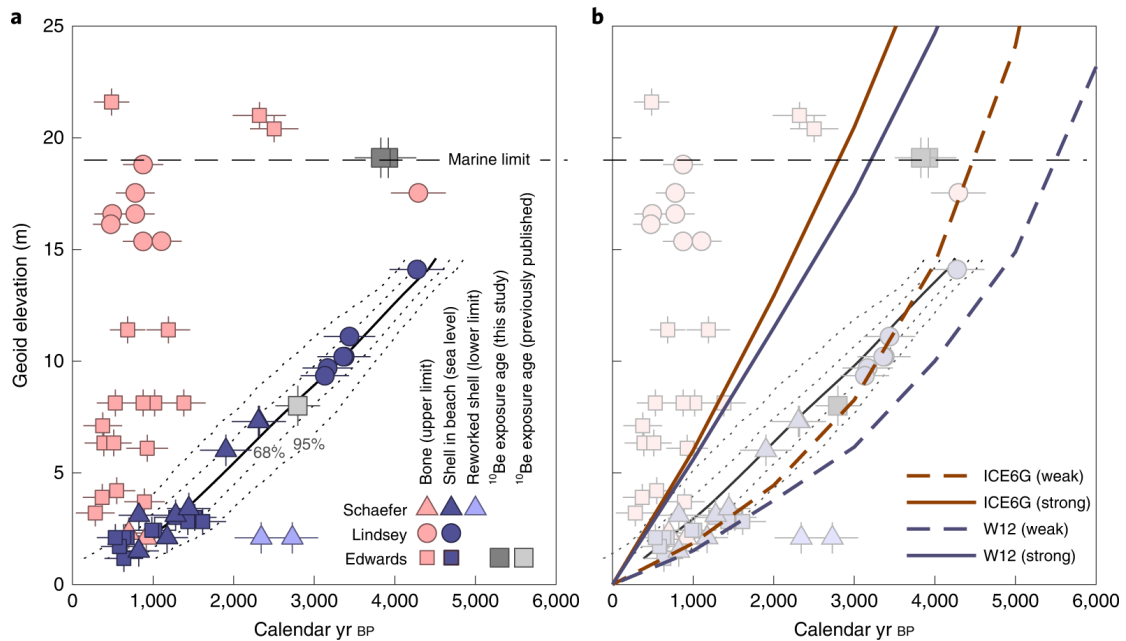


**Figure 2.** RSL reconstruction and comparison with GIA models for the Amundsen Sea Embayment, Antarctica. a, RSL curve based on radiocarbon ages of shells from raised beaches. All samples are presented as calibrated radiocarbon ages for shells and bones with horizontal bars indicating 2-sigma errors. The solid black line with associated bootstrap confidence intervals is an interpolation of the shell data (see Supplementary Information) using the method of ref. 37. The horizontal dashed black line represents the proposed regional marine limit (elevation of highest sampled beach) at 19 m. Elevation errors (Methods) associated with radiocarbon samples are represented by vertical bars on each data point and range from 0.3 to 0.7 m. Vertical error bars for Lindsey Island samples (0.3 m) are smaller than symbols at this scale. b, Comparison of RSL data with GIA model predictions derived using two different ice-history models (ICE-6G\_C27,32 and W1228,33). For each ice-history model, two curves are shown; these represent RSL change assuming either a strong (solid lines, upper mantle viscosity =  $5 \times 10^{20}$  Pa s) or a weak (dashed lines, upper mantle viscosity =  $5 \times 10^{19}$  Pa s) Earth model. The lithosphere thickness is set at 71 km (ref. 34).

## 10. 格陵兰 EastGRIP 冰芯的融化揭示了全新世温暖事件



翻译人：刘宇星 11811211@mail.sustech.edu.cn

Westhoff J, Sinnl G, Svensson A, et al. *Melt in the Greenland EastGRIP ice core reveals Holocene warm events*[J]. *Climate of the Past*, 2022, 18(5): 1011-1034.

<https://doi.org/10.5194/cp-18-1011-2022>

**摘要：**我们提供了从格陵兰岛东北部的东格陵兰冰芯项目(EastGRIP)获得的冰芯融化事件记录，涵盖了全新世的大部分时间。使用光学暗场线性扫描仪获取数据。我们检测并描述了整个气泡插合物过渡带上方冰芯中的融化层和透镜体（亦被称为无气泡层和透镜体）。这一转变位于 EastGRIP 冰芯 1150 m 深度，对应的年龄为 9720 年 b2k。我们将 EastGRIP 冰芯中的脆性区定义为 650 至 950 m 深度的区域，平均每米有超过 3 个冰芯断裂处。我们分析融化层厚度，矫正冰减薄效应，并解释由于冰芯破裂而导致的缺失层。我们对融化事件的记录显示，大约 1014 年 b2k (986 CE)有一个大而明显的峰，大约 7000 年 b2k 有一个宽峰，对应于全新世气候适宜期。总的来说，我们可以识别过去 10000 年中大约 831 mm 的融化体（针对冰减薄进行了校正）。我们发现 986 CE 的融化事件很可能是与 2012 CE 相似的强降水事件，并且这两个事件在整个全新世都是前所未有的。我们还将近 2500 年的冰芯数据与年轮数据进行了比较，发现融化事件和年轮异常之间存在重叠，表明夏季温暖。我们指出，考虑到由东北格陵兰冰流(NEGIS)的流动导致影响了 EastGRIP 站点的冰动力学，在全新世早期相比于现代夏季温度必须至少升高  $3 \pm 0.6^\circ\text{C}$ 。

**ABSTRACT:** We present a record of melt events obtained from the East Greenland Ice Core Project (EastGRIP) ice core in central northeastern Greenland, covering the largest part of the Holocene. The data were acquired visually using an optical dark-field line scanner. We detect and describe melt layers and lenses, seen as bubble-free layers and lenses, throughout the ice above the bubble-clathrate transition. This transition is located at 1150 m depth in the EastGRIP ice core, corresponding to an age of 9720 years b2k. We define the brittle zone in the EastGRIP ice core as that from 650 to 950 m depth, where we count on average more than three core breaks per meter.

We analyze melt layer thicknesses, correct for ice thinning, and account for missing layers due to core breaks. Our record of melt events shows a large, distinct peak around 1014 years b2k (986 CE) and a broad peak around 7000 years b2k, corresponding to the Holocene Climatic Optimum. In total, we can identify approximately 831 mm of melt (corrected for thinning) over the past 10 000 years. We find that the melt event from 986 CE is most likely a large rain event similar to that from 2012 CE, and that these two events are unprecedented throughout the Holocene. We also compare the most recent 2500 years to a tree ring composite and find an overlap between melt events and tree ring anomalies indicating warm summers. Considering the ice dynamics of the EastGRIP site resulting from the flow of the Northeast Greenland Ice Stream (NEGIS), we find that summer temperatures must have been at least  $3 \pm 0.6$  °C warmer during the Early Holocene compared to today.

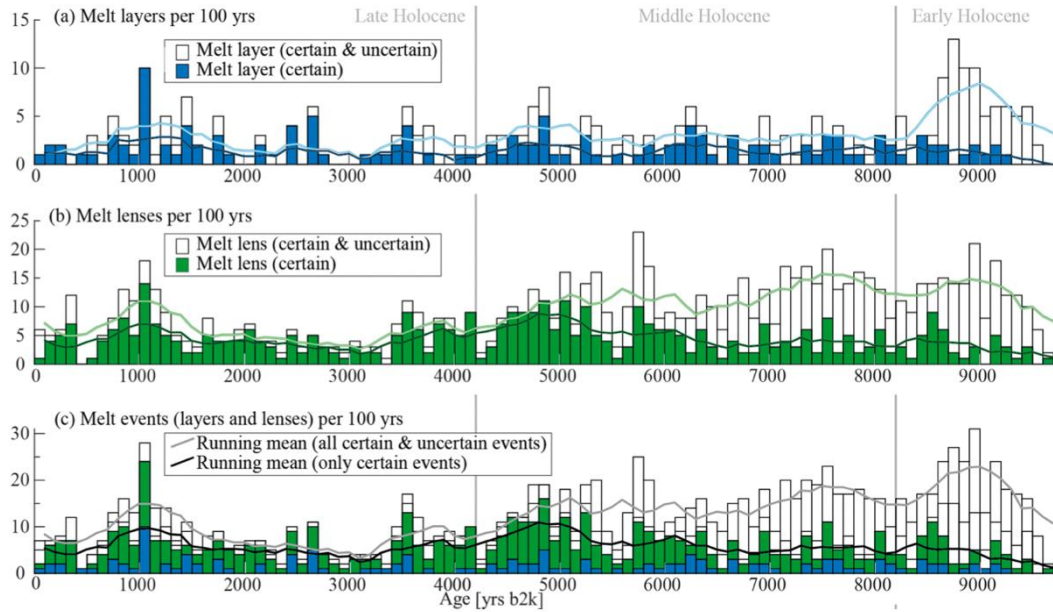


**Figure 1.** Number of melt layers and lenses per century throughout the last 9700 years in the EastGRIP ice core. Running means are shown as solid lines. (a) Melt layers (dark blue) and uncertain melt layers (white). (b) Melt lenses (dark green) and uncertain melt lenses (white). (c) Melt events, i.e., panels (a) and (b) stacked, including their uncertainties. Note that the bar representing the period from 0 to 100 years b2k represents only 56 years, not 100 years like the other bars, as our analysis begins in 1956 CE.

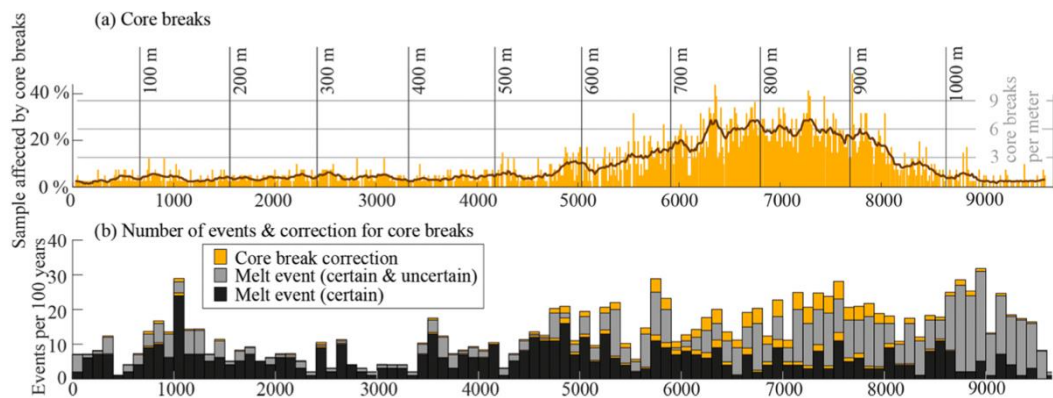


**Figure 2.** (a) Percentage of a 165 cm sample affected by core breaks (orange bars, scale on the left side), number of core breaks per meter (orange bars, scale on the right side), and running mean over 16.5 m (brown line). The broad peak between 650 and 950 m depth indicates the brittle zone. (b) Certain melt events (black) and uncertain melt events (gray) corrected for potentially missed events in the proximity of core breaks (orange).

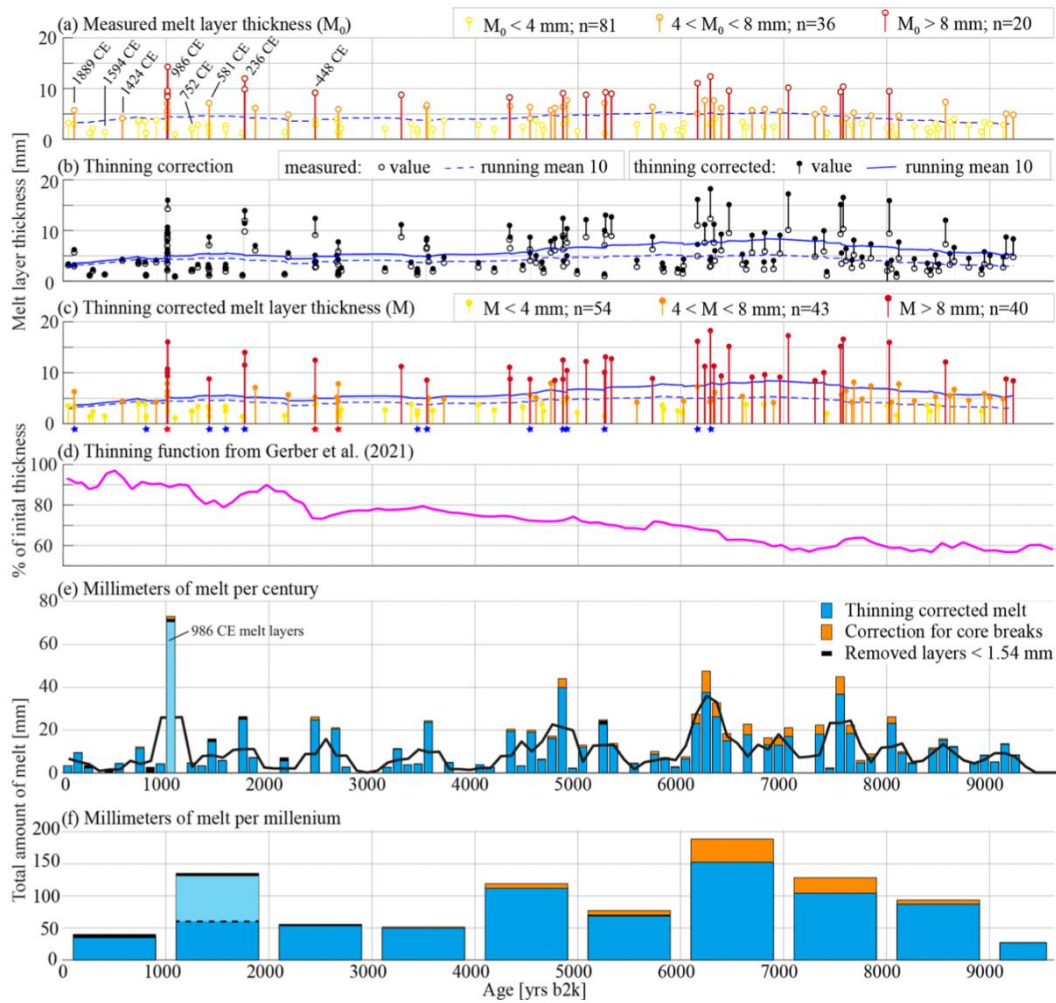


**Figure 3.** The layer thicknesses of melt layers are shown by the yellow, orange, and red bars (smaller than 4 mm, between 4 and 8 mm, and greater than 8 mm, respectively). To distinguish events occurring within a short period, the layer thicknesses are indicated by circles (measured thicknesses  $M_0$  are indicated by open circles, and thinning-corrected thicknesses  $M$  are indicated by closed circles). Running means of 10 events are indicated by dashed (for measured thicknesses) and solid (for thinning-corrected thicknesses) blue lines. Panel (a) shows events that were later compared to tree rings, along with their dates in CE notation. (b) Individual layer thicknesses corrected for thinning using the thinning function from Gerber et al. (2021) shown in (d). Stars in (c) mark multiple events within 5-year periods (blue stars indicate two events, red stars indicate three or more). Panels (e) and (f) show the millimeters of melt (blue bars, calculated from melt layer thicknesses) per century (e) and millennium (f), potentially missed events due to core breaks (orange), removed layers smaller than 1.54 mm (black), and the running mean (black line). Melt layers around the year 986 CE are plotted in light blue.